Long-range interaction coefficients for ytterbium dimers

S. G. Porsev,[1,2] M. S. Safronova,[1,3] A. Derevianko,[4] and Charles W. Clark[3]
[1]*Department of Physics and Astronomy, University of Delaware, Newark, Delaware 19716, USA*
[2]*Petersburg Nuclear Physics Institute, Gatchina, Leningrad District, 188300, Russia*
[3]*Joint Quantum Institute, National Institute of Standards and Technology and the University of Maryland, Gaithersburg, Maryland 20899, USA*
[4]*Physics Department, University of Nevada, Reno, Nevada 89557, USA*
(Received 9 July 2013; published 24 January 2014)

We evaluate the electric-dipole and electric-quadrupole static and dynamic polarizabilities for the $6s^2\,{}^1S_0$, $6s6p\,{}^3P_0^o$, and $6s6p\,{}^3P_1^o$ states and estimate their uncertainties. A first-principles relativistic method is developed for an accurate calculation of the van der Waals coefficients of dimers involving excited-state atoms with strong decay channel to the ground state. This method is used for evaluation of the long-range interaction coefficients of particular experimental interest, including the C_6 coefficients for the Yb-Yb ${}^1S_0 + {}^3P_{0,1}^o$ and ${}^3P_0^o + {}^3P_0^o$ dimers and C_8 coefficients for the ${}^1S_0 + {}^1S_0$ and ${}^1S_0 + {}^3P_1^o$ dimers.

DOI: 10.1103/PhysRevA.89.012711 PACS number(s): 34.20.Cf, 32.10.Dk, 31.15.ac

I. INTRODUCTION

The ytterbium atom has two fermionic and five bosonic isotopes, a ${}^1S_0$ ground state, a long-lived metastable $6s6p\ {}^3P_0^o$ state, and transitions at convenient wavelengths for laser cooling and trapping. All this makes Yb a superb candidate for a variety of applications such as development of optical atomic clocks [1], study of degenerate quantum gases [2], quantum information processing [3], and studies of fundamental symmetries [4]. The best limit to date on the value of the electron electric-dipole moment (EDM) which constrains extensions of the standard model of electroweak interactions was obtained using the YbF molecule [5]. YbRb and YbCs molecules have also been proposed for searches for the electron EDM [6] since they can be cooled to very low temperatures and trapped in optical dipole traps, leading to very long coherence times in comparison to molecular beam EDM experiments.

Yb is of particular interest for studying quantum gas mixtures [2,7–15]. Significant progress has been achieved in studying the properties of Yb-Yb photoassociation spectra at ultralow temperatures [7]. Photoassociation spectroscopy has been performed on bosons [2,8] and fermions [9]. The use of optical Feshbach resonances for control of entangling interactions between nuclear spins of ^{171}Yb atoms for quantum information processing applications has been proposed in Ref. [16]. A p-wave optical Feshbach resonance using purely long-range molecular states of a fermionic isotope of ytterbium ^{171}Yb was demonstrated in Ref. [11]. Recent work [17] theorizes that the case of ^{174}Yb may have sufficiently small direct background interaction between the atoms to support two bound states that represent attractively and repulsively bound dimers occurring simultaneously.

The excited molecular states asymptotically connected to the ${}^1S_0 + {}^3P_1^o$ separated Yb atom limit were investigated by Takasu *et al.* in Ref. [12]. They reported the successful production of a subradiant 1_g state of a two-atom Yb system in a three-dimensional optical lattice. The properties of the long-range potential were studied and the van der Waals coefficients C_3, C_6, and C_8 were predicted. However, fit of the C_6 and C_8 coefficients for the 1_g state was rather uncertain, with strong correlation between the C_6 and C_8 fit parameters [18].

Knowledge of the C_6 and C_8 long-range interaction coefficients in Yb-Yb dimers is critical to understanding the physics of dilute gas mixtures. Recently, we evaluated the C_6 coefficient for the Yb-Yb ${}^1S_0 + {}^1S_0$ dimer and found it to be $C_6 = 1929(39)$ [19], in excellent agreement with the experimental result $C_6 = 1932(35)$ [10]. However, the same method can not be directly applied to the calculation of the van der Waals coefficients with Yb-Yb ${}^1S_0 + {}^3P_1^o$ dimer owing to the presence of the ${}^3P_1^o \to {}^1S_0$ decay channel.

In this work, we develop the relativistic methodology for an accurate calculation of the van der Waals coefficients of dimers involving excited-state atoms with a strong decay channel to the ground state and evaluate C_6 and C_8 coefficients of particular experimental interest. The nonrelativistic formalism has been described in Refs. [20–22]. We carefully study the uncertainties of all quantities calculated in this work so the present values can be reliably used to analyze existing measurements and to facilitate planning of the future experimental studies. The methodology developed in this work can be used for evaluation of van der Waals coefficients in a variety of systems.

II. GENERAL FORMALISM

We investigate the molecular potentials asymptotically connecting to the $|A\rangle + |B\rangle$ atomic states. The wave function of such a system constructed from these states is

$$|M_A, M_B; \Omega\rangle = |A\rangle_{\rm I}\,|B\rangle_{\rm II}, \tag{1}$$

where the index I (II) describes the wave function located on the center I (II) and $\Omega = M_A + M_B$. Here, the $M_{A(B)}$ is the projection of the appropriate total atomic angular momentum $\mathbf{J}_{A(B)}$ on the internuclear axis. We assume that Ω is a good quantum number for all calculations in this work [Hund's case (c)].

The molecular wave functions can be obtained by diagonalizing the molecular Hamiltonian

$$\hat{H} = \hat{H}_A + \hat{H}_B + \hat{V}(R) \tag{2}$$

in the model space. Here, $\hat{H}_A$ and $\hat{H}_B$ represent the Hamiltonians of the two noninteracting atoms and $\hat{V}(R)$ is the

residual electrostatic potential defined as the full Coulomb interaction energy in the dimer excluding interactions of the atomic electrons with their parent nuclei.

Unless stated otherwise, throughout this paper we use atomic units (a.u.); the numerical values of the elementary charge $|e|$, the reduced Planck constant $\hbar = h/2\pi$, and the electron mass m_e are set equal to 1. The atomic unit for polarizability can be converted to SI units via α/h [Hz/(V/m)^2] = $2.48832 \times 10^{-8}\alpha$ (a.u.), where the conversion coefficient is $4\pi\epsilon_0 a_0^3/h$, a_0 is the Bohr radius, and ϵ_0 is the dielectric constant.

The potential $V(R)$ may be expressed as an expansion in the multipole interactions:

$$V(R) = \sum_{l,L=0}^{\infty} V_{lL}/R^{l+L+1},$$

where V_{lL} are given by [23]

$$V_{lL}(R) = \sum_{\mu=-l_s}^{l_s} \frac{(-1)^L (l+L)!}{\{(l-\mu)!\,(l+\mu)!\,(L-\mu)!\,(L+\mu)!\}^{1/2}} \times \left(T_\mu^{(l)}\right)_{\rm I} \left(T_{-\mu}^{(L)}\right)_{\rm II}. \quad (3)$$

Here, $l_s = \min(l, L)$ and the multipole spherical tensors are

$$T_\mu^{(K)} = -\sum_i r_i^K C_\mu^{(K)}(\hat{\mathbf{r}}_i), \quad (4)$$

where the summation is over atomic electrons, $\mathbf{r}_i$ is the position vector of electron i, and $C_\mu^{(L)}(\hat{\mathbf{r}}_i)$ are the reduced spherical harmonics [24].

We now restrict our consideration to the dipole-dipole and dipole-quadrupole interactions. Introducing designations $d_\mu \equiv T_\mu^{(1)}$, $Q_\mu \equiv T_\mu^{(2)}$, $V_{dd} \equiv V_{11}/R^3$, and $V_{dq} \equiv V_{12}/R^4$, we obtain from Eq. (3)

$$V_{dd}(R) = -\frac{1}{R^3}\sum_{\mu=-1}^{1} w_\mu^{(1)} (d_\mu)_{\rm I} (d_{-\mu})_{\rm II},$$
$$V_{dq}(R) = \frac{1}{R^4}\sum_{\mu=-1}^{1} w_\mu^{(2)} [(d_\mu)_{\rm I} (Q_{-\mu})_{\rm II} - (Q_\mu)_{\rm I} (d_{-\mu})_{\rm II}], \quad (5)$$

where the dipole and quadrupole weights are

$$w_\mu^{(1)} \equiv 1 + \delta_{\mu 0},$$
$$w_\mu^{(2)} \equiv \frac{6}{\sqrt{(1-\mu)!\,(1+\mu)!\,(2-\mu)!\,(2+\mu)!}}. \quad (6)$$

Numerically, $w_{-1}^{(2)} = w_{+1}^{(2)} = \sqrt{3}$ and $w_0^{(2)} = 3$.

The energy $\mathcal{E} \equiv E_A + E_B$, where E_A and E_B are the atomic energies of the $|A\rangle$ and $|B\rangle$ states, is obtained from

$$(\hat{H}_A + \hat{H}_B)|M_A, M_B; \Omega\rangle = \mathcal{E}\,|M_A, M_B; \Omega\rangle. \quad (7)$$

The molecular wave function $\Psi_\Omega^{g/u}$ can be formed as a linear combination of the wave functions given by Eq. (1). $\Psi_\Omega^{g/u}$ poses a definite gerade or ungerade symmetry and definite quantum number Ω. It can be represented by

$$\Psi_\Omega^p = \begin{cases} \frac{1}{\sqrt{2}}(|A\rangle_{\rm I}\,|B\rangle_{\rm II} + (-1)^p |B\rangle_{\rm I} |A\rangle_{\rm II}), & A \neq B \\ |A\rangle_{\rm I}\,|A\rangle_{\rm II}, & A = B \end{cases} \quad (8)$$

where we set $p = 0$ for ungerade symmetry and $p = 1$ for gerade symmetry. We have taken into account that the states A and B that are of interest to this work are the opposite parity states of Yb atom (when $A \neq B$).

Applying the formalism of Rayleigh-Schrödinger perturbation theory in the second order [25] and keeping the terms up to $1/R^8$ in the expansion of $V(R)$, we obtain the dispersion potential in two-atom basis:

$$U(R) \equiv \langle \Psi_\Omega^p | V(R) | \Psi_\Omega^p \rangle \approx \langle \Psi_\Omega^p | \hat{V}_{dd} | \Psi_\Omega^p \rangle + \sum_{\Psi_i \neq \Psi_\Omega^p} \left[\frac{\langle \Psi_\Omega^p | \hat{V}_{dd} | \Psi_i \rangle \langle \Psi_i | \hat{V}_{dd} | \Psi_\Omega^p \rangle}{\mathcal{E} - E_i} + \frac{\langle \Psi_\Omega^p | \hat{V}_{dq} | \Psi_i \rangle \langle \Psi_i | \hat{V}_{dq} | \Psi_\Omega^p \rangle}{\mathcal{E} - E_i} \right]. \quad (9)$$

The intermediate molecular state $|\Psi_i\rangle$ with unperturbed energy E_i runs over a *complete* set of two-atom states, excluding the model-space states, Eq. (1). The dispersion potential can be approximated as

$$U(R) \approx -\frac{C_3}{R^3} - \frac{C_6}{R^6} - \frac{C_8}{R^8}. \quad (10)$$

A. First-order corrections

The first-order correction, which is determined by the first term on the right-hand side of Eq. (9), is associated with the C_3 coefficient in Eq. (10). For the states considered in this work, this coefficient is nonzero only for the molecular potential asymptotically connecting to the $^1S_0 + {}^3P_1^o$ atomic states. It depends entirely on the reduced matrix element (ME) of the electric-dipole operator $|\langle {}^3P_1^o || d || {}^1S_0 \rangle|$ and is given by a simple formula

$$C_3(\Omega_p) = (-1)^{p+\Omega}(1 + \delta_{\Omega,0}) \frac{|\langle {}^3P_1^o || d || {}^1S_0 \rangle|^2}{3}. \quad (11)$$

Specifically,

$$C_3(0_{g/u}) = \mp 2 \frac{|\langle {}^3P_1^o || d || {}^1S_0 \rangle|^2}{3},$$
$$C_3(1_{g/u}) = \pm \frac{|\langle {}^3P_1^o || d || {}^1S_0 \rangle|^2}{3}, \quad (12)$$

where the upper (lower) sign corresponds to gerade (ungerade) symmetry.

B. Second-order corrections

The second-order corrections, associated with the C_6 and C_8 coefficients, are given by the second and third terms on the right-hand side of Eq. (9):

$$-\frac{C_6(\Omega_p)}{R^6} = \sum_{\Psi_i \neq \Psi_{\Omega_p}} \frac{\langle \Psi_{\Omega_p} | \hat{V}_{dd} | \Psi_i \rangle \langle \Psi_i | \hat{V}_{dd} | \Psi_{\Omega_p} \rangle}{\mathcal{E} - E_i},$$
$$-\frac{C_8(\Omega_p)}{R^8} = \sum_{\Psi_i \neq \Psi_{\Omega_p}} \frac{\langle \Psi_{\Omega_p} | \hat{V}_{dq} | \Psi_i \rangle \langle \Psi_i | \hat{V}_{dq} | \Psi_{\Omega_p} \rangle}{\mathcal{E} - E_i},$$

where $\mathcal{E} = E_A + E_B$ and the complete set of doubled atomic states satisfies the condition

$$\sum_{\Psi_i} |\Psi_i\rangle\langle\Psi_i| = 1.$$

After angular reduction, the C_6 coefficient can be expressed as

$$C_6(\Omega) = \sum_{J_\alpha=|J_A-1|}^{J_A+1} \sum_{J_\beta=|J_B-1|}^{J_B+1} A_{J_\alpha J_\beta}(\Omega)\, X_{J_\alpha J_\beta}, \tag{13}$$

where

$$A_{J_\alpha J_\beta}(\Omega) = \sum_{\mu M_\alpha M_\beta} \left[w_\mu^{(1)} \begin{pmatrix} J_A & 1 & J_\alpha \\ -M_A & \mu & M_\alpha \end{pmatrix} \times \begin{pmatrix} J_B & 1 & J_\beta \\ -M_B & -\mu & M_\beta \end{pmatrix} \right]^2,$$

$$X_{J_\alpha J_\beta} = \sum_{\alpha,\beta\neq A,B} \frac{|\langle A||d||\alpha\rangle|^2\, |\langle B||d||\beta\rangle|^2}{E_\alpha - E_A + E_\beta - E_B} \tag{14}$$

with fixed J_α and J_β.

If A and B are the spherically symmetric atomic states and there are no downward transitions from either of them, the C_6 and C_8 coefficients for the $A+B$ dimers are given by well-known formulas (see, e.g., [26])

$$\begin{aligned} C_6^{AB} &= C^{AB}(1,1), \\ C_8^{AB} &= C^{AB}(1,2) + C^{AB}(2,1), \end{aligned} \tag{15}$$

where the coefficients $C^{AB}(l,L)$ $(l,L=1,2)$ are quadratures of electric-dipole $\alpha_1(i\omega)$ and electric-quadrupole $\alpha_2(i\omega)$ dynamic polarizabilities at an imaginary frequency:

$$\begin{aligned} C^{AB}(1,1) &= \frac{3}{\pi}\int_0^\infty \alpha_1^A(i\omega)\,\alpha_1^B(i\omega)\,d\omega, \\ C^{AB}(1,2) &= \frac{15}{2\pi}\int_0^\infty \alpha_1^A(i\omega)\,\alpha_2^B(i\omega)\,d\omega, \\ C^{AB}(2,1) &= \frac{15}{2\pi}\int_0^\infty \alpha_2^A(i\omega)\,\alpha_1^B(i\omega)\,d\omega. \end{aligned} \tag{16}$$

For the Yb-Yb $^1S_0 + {}^3P_1^o$ dimer considered in this work, the expressions for C_6 and C_8 are more complicated due to the angular dependence, the $^3P_1^o \to {}^1S_0$ decay channel, and nonvanishing quadrupole moment of the $^3P_1^o$ state. After some transformations, we arrive at the following expression for the C_6 coefficient in the $^1S_0 + {}^3P_1^o$ case:

$$C_6(\Omega_p) = \sum_{J=0}^{2} A_J(\Omega) X_J, \tag{17}$$

where the angular dependence $A_J(\Omega)$ is represented by

$$A_J(\Omega) = \frac{1}{3}\sum_{\mu=-1}^{1} \left\{ w_\mu^{(1)} \begin{pmatrix} 1 & 1 & J \\ -\Omega & -\mu & \Omega+\mu \end{pmatrix} \right\}^2 \tag{18}$$

with the dipole weights $w_\mu^{(1)}$ given by Eq. (6) and $\Omega = 0,1$. It is worth noting that $A_J(\Omega)$ (and, consequently, the C_6 coefficients) do not depend on gerade or ungerade symmetry.

The quantities X_J for the $^1S_0 + {}^3P_1^o$ dimer are given by

$$X_J = \frac{27}{2\pi}\int_0^\infty \alpha_1^A(i\omega)\,\alpha_{1J}^B(i\omega)\,d\omega + \delta X_0\,\delta_{J,0}, \tag{19}$$

where $A \equiv {}^1S_0$ and $B \equiv {}^3P_1^o$ and δX_0 is defined below. The possible values of the total angular momentum J are 0, 1, and 2; $\alpha_1^A(i\omega)$ is the electric-dipole dynamic polarizability of the $^1S_0$ state at the imaginary argument.

The quantity $\alpha_{KJ}^\Phi(i\omega)$ is a part of the scalar electric-dipole $(K=1)$ or electric-quadrupole $(K=2)$ dynamic polarizability of the state Φ, in which the sum over the intermediate states $|n\rangle$ is restricted to the states with fixed total angular momentum $J_n = J$:

$$\alpha_{KJ}^\Phi(i\omega) \equiv \frac{2}{(2K+1)(2J_\Phi+1)} \times \sum_{\gamma_n} \frac{(E_n - E_\Phi)\,|\langle\gamma_n, J_n = J||T^{(K)}||\gamma_\Phi, J_\Phi\rangle|^2}{(E_n - E_\Phi)^2 + \omega^2}. \tag{20}$$

Here, γ_n stands for all quantum numbers of the intermediate states except J_n.

The correction δX_0 to the X_0 term in Eq. (19) is due to a downward $^3P_1^o \to {}^1S_0$ transition and is given by the following expression:

$$\delta X_0 = 2\,\left|\langle {}^3P_1^o||d||{}^1S_0\rangle\right|^2 \sum_{n\neq {}^3P_1^o} \frac{\left(E_n - E_{^1S_0}\right)\,|\langle n||d||{}^1S_0\rangle|^2}{\left(E_n - E_{^1S_0}\right)^2 - \omega_0^2} + \frac{\left|\langle {}^3P_1^o||d||{}^1S_0\rangle\right|^4}{2\omega_0}, \tag{21}$$

where $\omega_0 \equiv E_{^3P_1^o} - E_{^1S_0}$. The expression for the $C_8(^1S_0 + {}^3P_1^o)$ coefficient is substantially more complicated, so it is discussed in the Appendix.

III. METHOD OF CALCULATION

All calculations were carried out by two methods, which allows us to estimate the accuracy of the final values. The first method combines configuration interaction (CI) with many-body perturbation theory (MBPT) [27]. In the second method, which is more accurate, CI is combined with the coupled-cluster all-order approach (CI+all-order) that treats both core and valence correlation to all orders [28–30].

In both cases, we start from a solution of the Dirac-Fock (DF) equations for the appropriate states of the individual atoms,

$$\hat{H}_0\,\psi_c = \varepsilon_c\,\psi_c,$$

where H_0 is the relativistic DF Hamiltonian [27,29] and ψ_c and ε_c are single-electron wave functions and energies. The calculation was performed in the V^{N-2} approximation, i.e., the self-consistent procedure was done for the $[1s^2,\ldots,4f^{14}]$ closed core. The B-spline basis set, consisting of $N=35$ orbitals for each of partial wave with $l \leqslant 5$, was formed in a

spherical cavity with radius 60 a.u. The CI space is effectively complete. It includes the following orbitals: $6-20s, 6-20p$, $5-19d, 5-18f$, and $5-11g$.

The wave functions and the low-lying energy levels are determined by solving the multiparticle relativistic equation for two valence electrons [31]

$$H_{\rm eff}(E_n)\Phi_n = E_n\Phi_n. \tag{22}$$

The effective Hamiltonian is defined as

$$H_{\rm eff}(E) = H_{\rm FC} + \Sigma(E), \tag{23}$$

where $H_{\rm FC}$ is the Hamiltonian in the frozen-core approximation. The energy-dependent operator $\Sigma(E)$ which takes into account virtual core excitations is constructed using the second-order perturbation theory in the CI+MBPT method [27] and using linearized coupled-cluster single-double method in the CI+all-order approach [29]. $\Sigma(E) = 0$ in the pure CI approach. Construction of the effective Hamiltonian in the CI+MBPT and CI+all-order approximations is described in detail in Refs. [27,29]. The contribution of the Breit interaction is negligible at the present level of accuracy and was omitted.

The dynamic polarizability of the 2^K-pole operator $T^{(K)}$ at imaginary argument is calculated as the sum of three contributions: valence, ionic core, and vc. The vc term subtracts out the ionic core terms which are forbidden by the Pauli principle. Then,

$$\alpha_K(i\omega) = \alpha^v_K(i\omega) + \alpha^c_K(i\omega), \tag{24}$$

where both the core and vc parts are included in $\alpha^c_K(i\omega)$.

A. Valence contribution

The valence part of the dynamic polarizability $\alpha^v_K(i\omega)$ of an atomic state $|\Phi\rangle$ is determined by solving the inhomogeneous equation in the valence space. If we introduce the wave function of intermediate states $|\delta\Phi\rangle$ as

$$\begin{aligned}|\delta\Phi\rangle &\equiv {\rm Re}\left\{\frac{1}{H_{\rm eff}-E_\Phi+i\omega}\sum_i|\Phi_i\rangle\langle\Phi_i|T^{(K)}_0|\Phi\rangle\right\}\\ &= {\rm Re}\left\{\frac{1}{H_{\rm eff}-E_\Phi+i\omega}T^{(K)}_0|\Phi\rangle\right\},\end{aligned} \tag{25}$$

where "Re" means the real part, then $\alpha^v(i\omega)$ is given by

$$\alpha^v(i\omega) = 2\,\langle\Phi|T^{(K)}_0|\delta\Phi\rangle. \tag{26}$$

Here, $T^{(K)}_0$ is the zeroth component of the $T^{(K)}$ tensor. We include random-phase approximation (RPA) corrections to the 2^K-pole operator $T^{(K)}_0$. Equations (25) and (26) can also be used to find α^v_{KJ}, i.e., the part of the valence polarizability, where summation goes over only the intermediate states with fixed total angular momentum J. We refer the reader to Ref. [32] for further details of this approach.

B. Core contribution

The core and vc contributions to multipole polarizabilities are evaluated in the single-electron relativistic RPA approximation. The small α^{vc} term is calculated by adding vc contributions from the individual electrons, i.e., $\alpha^{vc}(6s^2) = 2\,\alpha^{vc}(6s)$ and $\alpha^{vc}(6s6p) = \alpha^{vc}(6s) + \alpha^{vc}(6p)$.

A special consideration is required when we need to find the core contribution to $\alpha^\Phi_{KJ}(i\omega)$ of a state Φ. If we disregard possible excitations of the core electrons to the occupied valence shells, the valence and core subsystems can be considered as independent. Then, the total angular momenta $\mathbf{J}_\Phi$ and $\mathbf{J}_n$ of the states Φ and Φ_n, respectively, can be represented as the sum of the valence and core parts $\mathbf{J} = \mathbf{J}^v + \mathbf{J}^c$. In our consideration, the core of the Φ state consists of the closed shells, and $J^c_\Phi = 0$. If we assume that the electrons are excited from the core, while the valence part of the wave function remains the same, we can express the reduced matrix element of the operator $T^{(K)}$ as

$$\langle J_\Phi||T^{(K)}||J_n\rangle = \left\langle J^c_\Phi = 0, J^v_\Phi, J_\Phi\middle||T^{(K)}|\middle|J^c_n = K, J^v_\Phi, J_n\right\rangle. \tag{27}$$

If $T^{(K)}$ acts only on the core part of the system, we arrive at (see, e.g., [24])

$$\begin{aligned}&\left\langle J^c_\Phi = 0, J^v_\Phi, J_\Phi\middle||T^{(K)}|\middle|J^c_n = K, J^v_\Phi, J_n\right\rangle\\ &\quad= \sqrt{\frac{2J_n+1}{2K+1}}\left\langle J^c_\Phi = 0\middle||T^{(K)}|\middle|J^c_n = K\right\rangle.\end{aligned} \tag{28}$$

Then, using Eq. (20), we can write the core contribution to $\alpha_{KJ}(i\omega)$ of the Φ state as

$$\begin{aligned}\alpha^c_{KJ}(i\omega) = {}& \frac{2\,(2J+1)}{(2K+1)^2\,(2J_\Phi+1)}\\ &\times\sum_{\gamma^c_n}\frac{(E_n-E_\Phi)\left|\left\langle J^c_\Phi = 0\middle||T^{(K)}|\middle|J^c_n = K\right\rangle\right|^2}{(E_n-E_\Phi)^2+\omega^2}.\end{aligned} \tag{29}$$

Taking into account that the core polarizability $\alpha^c_K(i\omega)$ of the operator $T^{(K)}$ in a single-electron approximation can be written as

$$\alpha^c_K(i\omega) = \frac{2}{2K+1}\sum_{a,n}\frac{\varepsilon_n-\varepsilon_a}{(\varepsilon_n-\varepsilon_a)^2+\omega^2}|\langle n||T^{(K)}||a\rangle|^2, \tag{30}$$

where $|a\rangle$ and $|n\rangle$ are the single-electron core and virtual states, we arrive at

$$\alpha^c_{KJ}(i\omega) = \frac{2J+1}{(2K+1)(2J_\Phi+1)}\alpha^c_K(i\omega). \tag{31}$$

Finally, $\alpha_{KJ}(i\omega)$ of the Φ state can be approximated as

$$\alpha_{KJ}(i\omega) = \alpha^v_{KJ}(i\omega) + \frac{2J+1}{(2K+1)(2J_\Phi+1)}\alpha^c_K(i\omega), \tag{32}$$

where possible values of J are from $\min(0,|J_\Phi-K|)$ to $J_\Phi+K$.

IV. RESULTS AND DISCUSSION

A. Energy levels

We start from the calculation of the low-lying energy levels of atomic Yb. The calculations were carried out using CI, CI+MBPT, and CI+all-order methods. The results are listed in Table I (see also the Supplemental Material to Ref. [19]) in columns labeled "CI," "CI+MBPT," and "CI+All." Two-electron binding energies are given in the first row, energies in other rows are counted from the ground state. Corresponding

TABLE I. Theoretical and experimental [33] energy levels (in cm^{-1}). Two-electron binding energies are given in the first row, energies in other rows are counted from the ground state. Results of the CI, CI+MBPT, and CI+all-order calculations are given in columns labeled "CI," "CI+MBPT," and "CI+All." Corresponding relative differences of these three calculations with the experiment are given in cm^{-1} and in percentages.

					Differences (cm^{-1})			Differences (%)		
State	Expt.	CI	CI+MBPT	CI+All	CI	CI+MBPT	CI+all	CI	CI+MBPT	CI+All
$6s^2\,{}^1S_0$	148650	137648	150532	149751	−11003	1882	1101	−7.4	1.3	0.7
$5d6s\ {}^3D_1$	24489	25505	25301	25108	1016	812	619	4.1	3.3	2.5
$5d6s\ {}^3D_2$	24752	25522	25587	25368	770	835	616	3.1	3.4	2.5
$5d6s\ {}^3D_3$	25271	25597	26172	25891	326	901	620	1.3	3.6	2.5
$5d6s\ {}^1D_2$	27678	25944	28842	28353	−1734	1164	676	−6.3	4.2	2.4
$6s7s\ {}^3S_1$	32695	29631	33170	33092	−3064	475	397	−9.4	1.5	1.2
$6s7s\ {}^1S_0$	34351	31346	34848	34755	−3005	497	404	−8.7	1.4	1.2
$6s6p\ {}^3P^o_0$	17288	14032	18258	17760	−3256	969	472	–19	5.6	2.7
$6s6p\ {}^3P^o_1$	17992	14675	18949	18450	−3317	957	458	–18	5.3	2.5
$6s6p\ {}^3P^o_2$	19710	16137	20698	20251	−3574	987	541	–18	5.0	2.7
$6s6p\ {}^1P^o_1$	25068	23888	26461	25967	−1181	1393	899	−4.7	5.6	3.6
$6s7p\ {}^3P^o_0$	38091	34649	38672	38504	−3441	581	413	−9.0	1.5	1.1
$6s7p\ {}^3P^o_1$	38174	34736	38745	38572	−3438	571	398	−9.0	1.5	1.0
$6s7p\ {}^3P^o_2$	38552	35045	39127	38962	−3507	575	410	−9.1	1.5	1.1
$6s7p\ {}^1P^o_1$	40564	35697	39534	39311	−4867	−1030	−253	–12	−2.5	−3.1

relative differences of these three calculations with experiment are given in cm^{-1} and in percentages. The even- and odd-parity levels are schematically presented in Fig. 1.

Table I illustrates that the difference between the theory and the experiment is as large as 19% for the odd-parity states at the CI stage. When we include the core-core and core-valence correlations in the second order of the perturbation theory (CI+MBPT method), the accuracy significantly improves. Further improvement is achieved when we use the CI+all-order method including correlations in all orders of the MBPT.

B. Polarizabilities

In Table II, we give a breakdown of the main contributions from the intermediate states to the static electric-dipole and electric-quadrupole polarizabilities of the $6s^2\,{}^1S_0$, $6s6p\,{}^3P^o_0$, and $6s6p\,{}^3P^o_1$ states in the CI+all-order approximation. For the $^3P^o_1$ state, the contributions to the scalar parts of the polarizabilities are presented. While we do not explicitly use

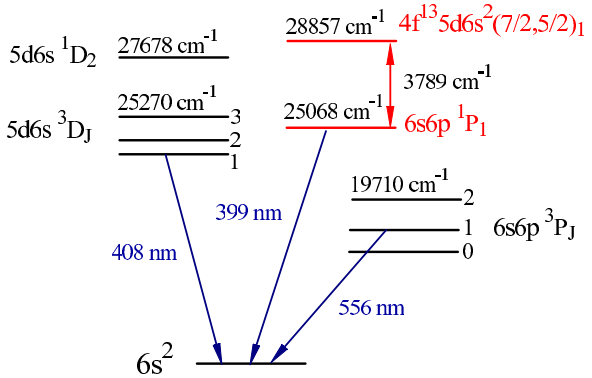

FIG. 1. (Color online) Low-lying energy levels of Yb. Other states of the $4f^{13}5d6s^2$ configuration are not shown.

the sum-over-states to calculate the polarizabilities, we can separately compute contributions of individual intermediate states. The row labeled "Other" lumps contributions of all other valence states not explicitly listed in the table. The row labeled "Core+vc" gives the contributions from the core and vc terms and the row labeled "Total" is the final value obtained as the sum of all contributions. The theoretical and experimental transition energies are presented in columns $\Delta E_{\rm theor}$ and $\Delta E_{\rm expt}$ (in cm^{-1}). We used the theoretical energies when calculating the contributions of the individual terms to the polarizabilities. These contributions as well as the total values of the polarizabilities are given in the column labeled "α."

The role of different contributions to the $6s6p\,{}^3P^o_0$ polarizability was analyzed in Ref. [19] (see the Supplemental Material). We compare the $^3P^o_0$ case with the contributions to the scalar part of the $^3P^o_1$ polarizability given in Table II. We find that the main contributions to the $6s6p\,{}^3P^o_0$ and $6s6p\,{}^3P^o_1$ polarizabilities are similar in every respect. In particular, the $5d6s\,{}^3D_J$ states contribute ∼57% to both polarizabilities. The contributions of the $6s6d\,{}^3D_J$ states are at the level of 7%–10%. The higher-excited states not explicitly listed in the table, labeled as "Other," contribute ∼21% in both cases.

To the best of our knowledge, there are no experimental data for the electric-quadrupole polarizabilities listed in the table or any transitions that give dominant contributions to α_2. For instance, the main contribution (76%) to $\alpha_2({}^1S_0)$ comes from the $5d6s\,{}^1D_2$ state. Any accurate experimental data for the $5d6s\,{}^1D_2$ state (lifetime, oscillator strengths, etc.) would provide an important benchmark relevant to the ground-state quadrupole polarizability.

We also give the breakdown of the $6s6p\,{}^3P^o_0$ and the scalar part of $6s6p\,{}^3P^o_1$ electric-quadrupole polarizabilities. The main contribution (80%) comes from the $6s6p\,{}^3P^o_2$ state in both cases. We note that the remainder contribution (listed in rows "Other") is significant for all polarizabilities considered

TABLE II. A breakdown of the contributions to the $6s^2\,{}^1S_0$, $6s6p\,{}^3P_0^o$, and $6s6p\,{}^3P_1^o$ electric-dipole α_1 and electric-quadrupole α_2 static polarizabilities in the CI+all-order approximation. For the ${}^3P_1^o$ state, the scalar polarizabilities are given. The row labeled "Other" gives the contribution of all other valence states not explicitly listed in the table. The row labeled "Core+vc" gives the contributions from the core and *vc* terms. The row labeled "Total" lists the final values obtained as the sum of all contributions. $|\langle n||T^{(K)}||m\rangle|$ are the reduced matrix elements; $T^{(1)} = d$ and $T^{(2)} = Q$ stand for the electric-dipole and electric-quadrupole operators, respectively. The theoretical and experimental transition energies are presented in columns $\Delta E_{\rm theor}$ and $\Delta E_{\rm expt}$ (in $\rm cm^{-1}$). The contributions to the polarizabilities are given in the column labeled "α."

Polariz.	Contrib.	$\lvert\langle n\rvert\rvert T^{(K)}\rvert\rvert m\rangle\rvert$	$\Delta E_{\rm theor}$	$\Delta E_{\rm expt}$	α
$\alpha_1({}^3P_0^o)$	$5d6s\,{}^3D_1$	2.89	7346	7201	166
	$6s7s\,{}^3S_1$	1.95	15332	15406	36
	$6s6d\,{}^3D_1$	1.84	22490	22520	22
	Other				63
	Core + vc				6
	Total				293
$\alpha_{1s}({}^3P_1^o)$	$6s^2\,{}^1S_0$	0.571	−18450	−17992	–1
	$5d6s\,{}^3D_1$	2.51	6656	6497	46
	$5d6s\,{}^3D_2$	4.35	6916	6760	133
	$5d6s\,{}^1D_2$	0.453	9899	9686	1
	$6s7s\,{}^3S_1$	3.46	14642	14703	40
	$6s7s\,{}^1S_0$	0.243	16305	16359	0.2
	$6s6d\,{}^3D_1$	1.62	21800	21817	6
	$6s6d\,{}^3D_2$	2.78	21831	21846	17
	$6s6d\,{}^1D_2$	0.614	22066	22070	1
	Other				66
	Core + vc				6
	Total				315
$\alpha_2({}^1S_0)$	$5d6s\,{}^3D_2$	3.00	25366	24752	31
	$5d6s\,{}^1D_2$	25.00	28349	27678	1936
	$6s6d\,{}^3D_2$	3.77	40281	39838	31
	$6s6d\,{}^1D_2$	8.06	40516	40062	141
	Other				407
	Core + vc				14
	Total				2559
$\alpha_2({}^3P_0^o)$	$6s6p\,{}^3P_2^o$	21.60	2490	2422	16449
	$6s7p\,{}^3P_2^o$	10.14	20202	21263	447
	Other				3691
	Core + vc				14
	Total				20602
$\alpha_{2s}({}^3P_1^o)$	$6s6p\,{}^3P_2^o$	32.69	1800	1718	17372
	$6s6p\,{}^1P_1^o$	5.62	7517	7076	123
	$6s7p\,{}^3P_1^o$	9.35	20122	20099	127
	$6s7p\,{}^3P_2^o$	16.30	20512	20560	379
	$6s7p\,{}^1P_1^o$	4.58	20861	22572	29
	Other				3973
	Core + vc				14
	Total				22017

here. These contributions are at the level of 15%–18%. The uncertainties of the polarizability values are discussed later in Sec. V.

TABLE III. The values of the $D \equiv |\langle 6s6p\,{}^3P_1^o||d||6s^2\,{}^1S_0\rangle|$ matrix element (in a.u.) and C_3 coefficients in the CI+MBPT and CI+all-order approximations.

	CI+MBPT	CI+all-order	Experiment
D	0.581	0.572	0.549(4)[a]
			0.5407(15)[b]
$C_3(0_u)$	0.225	0.218	0.1949(11)[b]
$C_3(0_g)$	−0.225	−0.218	
$C_3(1_u)$	−0.113	−0.109	
$C_3(1_g)$	0.113	0.109	0.09685[c]

[a]Reference [34]. The experimental number was obtained from the weighted ${}^3P_1^o$ lifetime $\tau({}^3P_1^o) = 845(12)$ ns.
[b]Reference [7] (this error is purely statistical).
[c]Reference [12].

C. C_3 coefficients

The values of the C_3 coefficients obtained in the CI+MBPT and CI+all-order approximations for the ${}^1S_0 + {}^3P_1^o$ dimer are given in Table III. We calculated the $|\langle 6s6p\,{}^3P_1^o||d||6s^2\,{}^1S_0\rangle|$ matrix element (ME) and then found C_3 coefficients using Eq. (12). The $C_3(0_g)$ and $C_3(1_u)$ have the same numerical values as $C_3(0_u)$ and $C_3(1_g)$, but the opposite sign. Our CI+all-order value for this ME differs from the experimental results by 4%–5%. It is not unexpected because the ${}^1S_0 - {}^3P_1^o$ transition is an intercombination transition and due to cancellation of different contributions its amplitude is relatively small. It may be also affected by the mixing with the core-excited states that are outside of our CI space as is discussed in detail in Ref. [19]. As a result, the accuracy of calculation of such MEs is lower. Using Eq. (12), we can estimate the accuracy of C_3 coefficients at the level of 8%–10%.

D. C_6 and C_8 coefficients

To find the van der Waals coefficients for the ${}^1S_0 + {}^3P_0^o$ and ${}^3P_0^o + {}^3P_0^o$ dimers, we computed the dynamic electric-dipole and electric-quadrupole polarizabilities of the ${}^1S_0$ and ${}^3P_0^o$ states at imaginary frequency and then used Eqs. (15) and (16). In practice, we computed the C_6^{AB} coefficients by approximating the integral (17) by Gaussian quadrature of the integrand computed on the finite grid of discrete imaginary frequencies [35]. The C_6 coefficient for the ${}^1S_0 + {}^1S_0$ dimer was obtained in Ref. [19].

The calculation of the C_6 and C_8 coefficients for the ${}^1S_0 + {}^3P_1^o$ dimer was carried out according to the expressions given by Eqs. (17)–(19) and in the Appendix. A breakdown of the contributions to the $C_6(\Omega)$ coefficient for Yb-Yb (${}^1S_0 + {}^3P_1^o$) dimer is given in Table IV. We list the quantities X_J and coefficients A_J given by Eqs. (18) and (19) for allowed $J = 0,1,2$. The δX_0 term is presented separately in the second row to illustrate the magnitude of this contribution. It is relatively small, 4% of the total for $\Omega = 0$ and 1% for $\Omega = 1$. It is included in the X_0 value given in the table. We note that the $C_6({}^1S_0 + {}^3P_1^o)$ coefficient does not depend on u/g symmetry. The CI+MBPT and CI+all-order values for X_J are given in columns labeled "MBPT" and "All." The relative differences between these values, which give an estimate of the higher-order contributions, are listed in the column labeled "HO." We

TABLE IV. A breakdown of the contributions to the $C_6(\Omega)$ coefficient for Yb-Yb ($^1S_0 + {}^3P_1^o$) dimer. The expressions for X_J and A_J are given by Eqs. (18) and (19). The δX_0 term is given separately in the second row; it is included in the $J = 0$ contribution. The CI+MBPT and CI+all-order values for X_J are given in columns labeled "MBPT" and "All."

	X_J			A_J		$C_6(\Omega)$	
J	MBPT	All	HO	$\Omega = 0$	$\Omega = 1$	$\Omega = 0$	$\Omega = 1$
0	1107	1135	2.5%	4/9	1/9	504	126
δ_0	248	253	2.0%	4/9	1/9	112	28
1	4564	4480	−1.9%	1/9	5/18	498	1244
2	6752	6702	−0.7%	11/45	19/90	1638	1415
Sum						2753	2814

find that the higher orders contribute with a different sign to $J = 0$ and $J = 1,2$.

A breakdown of the contributions to the $C_8(\Omega)$ coefficients for Yb-Yb $^1S_0 + {}^3P_1^o$ dimer is given in Table V. We list the quantities $X_k^{J_\alpha J_\beta}$ and coefficients $A_k^{J_\alpha J_\beta}$ (the analytical expressions for them are given in the Appendix). The δX_1^{11} and δX_2^{20} terms are given separately in the first and fifth rows; they are included in the X_1^{11} and X_2^{20} contributions, respectively. For calculation of δX_1^{11} we used the values $|\langle {}^3P_1^o||Q||{}^3P_1^o\rangle| = 17.75$ a.u. and the static $^1S_0$ polarizability $\alpha_1^A(0) = 140.9$ a.u. obtained in the CI+all-order approximation. The coefficients A_3^{11} and A_4^{22} contain $(-1)^p$, therefore, their sign is different for gerade and ungerade symmetry resulting in slightly different values for $C_8(\Omega_u)$ and $C_8(\Omega_g)$. In Table V, the + (−) sign corresponds to the ungerade (gerade) symmetry, respectively. The CI+all-order values are given for $X_k^{J_\alpha J_\beta}$ and C_8; the relative differences of the CI+all-order and CI+MBPT values are given in the column labeled "HO" in %.

Our final results for polarizabilities and the van der Waals C_6 and C_8 coefficients are summarized in Table VI. The $6s^2\,{}^1S_0$, $6s6p\,{}^3P_0^o$, and $6s6p\,{}^3P_1^o$ electric-dipole α_1 and electric-quadrupole α_2 static polarizabilities in the CI+MBPT and CI+all-order approximations are listed in a.u. For the $^3P_1^o$ state, the scalar parts of the polarizabilities are presented. The values of $C_6(\Omega_{u/g})$ and $C_8(\Omega_{u/g})$ coefficients for the $A + B$ dimers in the CI+MBPT and CI+all-order approximations are listed in the second part of the table. The (rounded) CI+all-order values are taken as final. The relative contribution of the higher-order corrections is estimated as the difference of the CI+all-order and CI+MBPT results; it is listed in column labeled "HO" in percent.

V. DETERMINATION OF UNCERTAINTIES

We compare frequency-dependent polarizabilities calculated in the CI+MBPT and CI+all-order approximations for all ω used in our finite grid to estimate the uncertainties of the C_6 and C_8 coefficients. We find that the difference between the CI+all-order and CI+MBPT frequency-dependent polarizability values is largest for $\omega = 0$ and decreases significantly with increasing ω. This is reasonable because for large ω the main contribution to the polarizability comes from its core part. But, the core parts are the same for both CI+all-order and CI+MBPT approaches.

Therefore, the fractional uncertainty $\delta C^{AB}(l,L)$ ($l,L = 1,2$) may be expressed via fractional uncertainties in the static multipole polarizabilities of the atoms A and B [39]:

$$\delta C^{AB}(l,L) = \sqrt{\left[\delta\alpha_l^A(0)\right]^2 + \left[\delta\alpha_L^B(0)\right]^2}. \tag{33}$$

The absolute uncertainties induced in C_6^{AB} and C_8^{AB} ($A \neq B$) are given by

$$\begin{aligned} \Delta C_6^{AB} &= \Delta C^{AB}(1,1), \\ \Delta C_8^{AB} &= \sqrt{[\Delta C^{AB}(1,2)]^2 + [\Delta C_{AB}(2,1)]^2}. \end{aligned} \tag{34}$$

TABLE V. A breakdown of the contributions to the $C_8(\Omega)$ coefficient for Yb-Yb ($^1S_0 + {}^3P_1^o$) dimer. The expressions for $X_k^{J_\alpha J_\beta}$ and $A_k^{J_\alpha J_\beta}$ are given in the Appendix. The δX_1^{11} term (designated as δ_1^{11}) is given separately in the first row; it is included in the X_1^{11} contribution. The δX_2^{20} term (designated as δ_2^{20}) is given separately in the fifth row; it is included in the X_2^{20} contribution. The CI+all-order values are given for $X_k^{J_\alpha J_\beta}$ and C_8; the relative differences of the CI+all-order and CI+MBPT values are given in columns labeled "HO" in %. The + (−) sign corresponds to the ungerade (gerade) symmetry, respectively.

			$A_k^{J_\alpha J_\beta}$		$C_8(\Omega)$	
$J_\alpha J_\beta, k$	$X_k^{J_\alpha J_\beta}$	HO	$\Omega = 0$	$\Omega = 1$	$\Omega = 0$	$\Omega = 1$
δ_1^{11}	66588	0.5%				
11,1	107772	0.0%	3/5	1/5	64663	21554
12,1	392687	−0.6%	1/15	7/15	26179	183254
13,1	249267	−1.1%	43/105	31/105	102081	73593
δ_2^{20}	6510	1.4%				
20,2	35061	3.5%	3/5	1/5	21037	7012
21,2	142845	−0.4%	1/5	2/5	28569	57138
22,2	213240	0.7%	9/25	8/25	76766	68237
11,3	1061	−5.6%	±3/5	±1/5	±637	±212
22,4	550	−15%	±9/25	±3/25	±198	±66
$C_8(\Omega_u)$					320130	411067
$C_8(\Omega_g)$					318461	410511

TABLE VI. The $6s^2\,{}^1S_0$, $6s6p\,{}^3P_0^o$, and $6s6p\,{}^3P_1^o$ electric-dipole α_1 and electric-quadrupole α_2 static polarizabilities in the CI+MBPT and CI+all-order approximations (in a.u.). For the ${}^3P_1^o$ state, the scalar parts of the polarizabilities are presented. The values of $C_6(\Omega_{u/g})$ and $C_8(\Omega_{u/g})$ coefficients for the $A+B$ dimers in the CI+MBPT and CI+all-order approximations are listed in the second part of the table. The (rounded) CI+all-order values are taken as final.

Level	Property	CI+MBPT	CI+all	HO	Final	Other
$6s^2\,{}^1S_0$	α_1[a]	138.3	140.9	1.8%	141(2)	141(6)[b]
						136.4(4.0)[c]
						144.59[d]
$6s6p\,{}^3P_0^o$	α_1[a]	305.9	293.2	−4.3%	293(10)	302(14)[b]
$6s6p\,{}^3P_1^o$	α_{1s}	323.3	315.3	−2.5%	315(11)	
$6s^2\,{}^1S_0$	α_2	2484	2559	2.9%	2560(80)	
$6s6p\,{}^3P_0^o$	α_2	21294	20601	−3.4%	20600(700)	
$6s6p\,{}^3P_1^o$	α_{2s}	22923	22017	−4.1%	22000(900)	
${}^1S_0+{}^1S_0$	C_6[a]	1901	1929	1.5%	1929(39)	1932(35)[e]
	C_8	182360	187860	2.9%	$1.88(6)\times10^5$	$1.9(5)\times10^5$[e]
${}^1S_0+{}^3P_0^o$	C_6	2609	2561	−1.9%	2561(95)	2709(338)[b]
${}^3P_0^o+{}^3P_0^o$	C_6	3916	3746	−4.5%	3746(180)	3886(360)[b]
${}^1S_0+{}^3P_1^o$	$C_6(0_{u/g})$	2649	2640	−0.3%	2640(103)	2410(220)[f]
	$C_6(1_{u/g})$	2824	2785	−1.4%	2785(109)	2283.6[g]
	$C_8(0_u)$	321097	320130	−0.3%	$3.20(14)\times10^5$	
	$C_8(1_u)$	412779	411067	−0.4%	$4.11(18)\times10^5$	
	$C_8(0_g)$	319300	318461	−0.3%	$3.18(14)\times10^5$	
	$C_8(1_g)$	412180	410511	−0.4%	$4.11(18)\times10^5$	

[a]Safranova *et al*. [19], theory.
[b]Dzuba and Derevianko [36], theory.
[c]Zhang and Dalgarno [37], based on experiment.
[d]Sahoo and Das [38], theory.
[e]Kitagawa *et al*. [10], experiment.
[f]Borkowski *et al*. [7], experiment; the error includes only uncertainty of the fit.
[g]Takasu *et al*. [12], experiment.

The polarizabilities and their absolute uncertainties are presented in Table VI. The uncertainties of the electric-dipole ${}^1S_0$ and ${}^3P_0^o$ polarizabilities were discussed in detail in Ref. [19]; the uncertainty of the ${}^3P_0^o$ polarizability was determined to be 3.4%. Table I illustrates that the accuracy of calculation of the ${}^3P_0^o$ and ${}^3P_1^o$ energy levels is practically the same (∼2.5% at the CI+all-order stage). We use the same method of solving the inhomogeneous equation to determine both the ${}^3P_0^o$ and ${}^3P_1^o$ polarizabilities. The main contributions to these polarizabilities are also very similar. Based on these arguments, we assume that the uncertainty of the scalar part of the ${}^3P_1^o$ polarizability can be estimated at the level of 3.5%.

Our estimates of the uncertainties of the electric-quadrupole polarizabilities are based on the differences between the CI+MBPT and CI+all-order values. Besides that, we take into account that in all cases the dominant contribution comes from the low-lying state which energies we reproduce well (see Table I). Based on the size of the higher-order correction, we assign the uncertainties 3%–4% to these polarizabilities. These results, as well as the final (recommended) values of the polarizabilities, are presented in Table VI.

Using Eqs. (33) and (34), we estimated the fractional uncertainties of the C_6 coefficient for the ${}^1S_0+{}^3P_{0,1}^o$ dimers at the level of 4%–4.5%. The uncertainty of the $C_8({}^1S_0+{}^1S_0)$ coefficient is 3.2% and the uncertainties of the $C_8({}^1S_0+{}^3P_1^o)$ coefficients are ∼4.5%. The difference of the CI+all-order and CI+MBPT values (4.5%) is taken as an uncertainty for the $C_6\,({}^3P_0^o+{}^3P_0^o)$ coefficient.

VI. CONCLUSION

To conclude, we evaluated the electric-dipole and electric-quadrupole static and dynamic polarizabilities for the $6s^2\,{}^1S_0$, $6s6p\,{}^3P_0^o$, and $6s6p\,{}^3P_1^o$ states and estimated their uncertainties. The C_6 and C_8 coefficients are evaluated for the Yb-Yb dimers. The uncertainties of our calculations of the van der Waals coefficients do not exceed 5%. Our result $C_8 = 1.88(6)\times10^5$ for the ${}^1S_0+{}^1S_0$ dimer is in excellent agreement with the experimental value $C_8 = 1.9(5)\times10^5$ [10]. The quantities calculated in this work allow future benchmark tests of molecular theory and experiment. Most of these quantities are determined for the first time. Methodology developed in this work can be used to evaluate properties of other dimers with excited atoms that have a strong decay channel.

ACKNOWLEDGMENTS

We thank P. Julienne for helpful discussions. This research was performed under the sponsorship of the US Department of Commerce, National Institute of Standards and Technology, and was supported by the National Science Foundation under Physics Frontiers Center Grant No. PHY-0822671 and by the Office of Naval Research. The work of S.G.P. was supported in part by US NSF Grant No. PHY-1212442 and RFBR Grant No. 11-02-00943. The work of A.D. was supported in part by the US NSF Grant No. PHY-1212482.

APPENDIX: C_8 COEFFICIENTS FOR THE $^1S_0 + {}^3P_1^o$ DIMER

Following the formalism of Sec. II, the C_8 coefficient may be expressed as

$$\frac{C_8(\Omega_p)}{R^8} = \sum_{A,B\neq\alpha,\beta} \frac{\langle AB|\hat{V}_{dq}|\alpha\beta\rangle\langle\alpha\beta|\hat{V}_{dq}|AB\rangle + (-1)^p\langle AB|\hat{V}_{dq}|\alpha\beta\rangle\langle\alpha\beta|\hat{V}_{dq}|BA\rangle}{E_\alpha + E_\beta - \mathcal{E}},$$

which can be further reduced to

$$C_8(\Omega_p) = \sum_{k=1}^{4}\sum_{J_\alpha J_\beta} A_k^{J_\alpha J_\beta}(\Omega_p) X_k^{J_\alpha J_\beta},$$

where

$$A_1^{J_\alpha J_\beta}(\Omega) = \sum_{\mu M_\alpha M_\beta}\left\{ w_\mu^{(2)} \begin{pmatrix} J_A & 1 & J_\alpha \\ -M_A & \mu & M_\alpha \end{pmatrix}\begin{pmatrix} J_B & 2 & J_\beta \\ -M_B & -\mu & M_\beta \end{pmatrix}\right\}^2, \quad X_1^{J_\alpha J_\beta} = \sum_{\alpha\beta}\frac{|\langle A||d||\alpha\rangle|^2|\langle B||Q||\beta\rangle|^2}{E_\alpha - E_A + E_\beta - E_B};$$

$$A_2^{J_\alpha J_\beta}(\Omega) = \sum_{\mu M_\alpha M_\beta}\left\{ w_\mu^{(2)} \begin{pmatrix} J_A & 2 & J_\alpha \\ -M_A & \mu & M_\alpha \end{pmatrix}\begin{pmatrix} J_B & 1 & J_\beta \\ -M_B & -\mu & M_\beta \end{pmatrix}\right\}^2, \quad X_2^{J_\alpha J_\beta} = \sum_{\alpha\beta}\frac{|\langle A||Q||\alpha\rangle|^2|\langle B||d||\beta\rangle|^2}{E_\alpha - E_A + E_\beta - E_B};$$

$$A_3^{J_\alpha J_\beta}(\Omega_p) = (-1)^p \sum_{\mu\lambda M_\alpha M_\beta}(-1)^{J_A - J_\alpha + J_B - J_\beta + 1} w_\mu^{(2)} w_\lambda^{(2)} \times \begin{pmatrix} J_A & 1 & J_\alpha \\ -M_A & \mu & M_\alpha \end{pmatrix}\begin{pmatrix} J_A & 1 & J_\beta \\ -M_A & \lambda & M_\beta \end{pmatrix}\begin{pmatrix} J_B & 2 & J_\beta \\ -M_B & -\mu & M_\beta \end{pmatrix}\begin{pmatrix} J_B & 2 & J_\alpha \\ -M_B & -\lambda & M_\alpha \end{pmatrix},$$

$$X_3^{J_\alpha J_\beta} = \sum_{\alpha\beta}\frac{\langle A||d||\alpha\rangle\langle\alpha||Q||B\rangle\langle B||Q||\beta\rangle\langle\beta||d||A\rangle}{E_\alpha - E_A + E_\beta - E_B};$$

$$A_4^{J_\alpha J_\beta}(\Omega_p) = (-1)^p \sum_{\mu\lambda M_\alpha M_\beta}(-1)^{J_A - J_\alpha + J_B - J_\beta + 1} w_\mu^{(2)} w_\lambda^{(2)} \times \begin{pmatrix} J_A & 2 & J_\alpha \\ -M_A & \mu & M_\alpha \end{pmatrix}\begin{pmatrix} J_A & 2 & J_\beta \\ -M_A & \lambda & M_\beta \end{pmatrix}\begin{pmatrix} J_B & 1 & J_\beta \\ -M_B & -\mu & M_\beta \end{pmatrix}\begin{pmatrix} J_B & 1 & J_\alpha \\ -M_B & -\lambda & M_\alpha \end{pmatrix},$$

$$X_4^{J_\alpha J_\beta} = \sum_{\alpha\beta}\frac{\langle A||Q||\alpha\rangle\langle\alpha||d||B\rangle\langle B||d||\beta\rangle\langle\beta||Q||A\rangle}{E_\alpha - E_A + E_\beta - E_B}.$$

The total angular momenta J_α and J_β of the intermediate states α and β are fixed in all of the equations above.

We are interested in the case when $A \equiv {}^1S_0$ and $B \equiv {}^3P_1^o$. Then, $J_A = 0$, $J_B = 1$, and $\Omega = M_B = 0,1$. For $k = 1$, we have $J_\alpha = 1$ and $J_\beta = 1,2,3$. The coefficients $A_1^{1J_\beta}(\Omega)$ are listed in Table V. The quantities $X_1^{1J_\beta}$ are given by

$$\begin{aligned} X_1^{1J_\beta} &= \frac{45}{2\pi}\int_0^\infty \alpha_1^A(i\omega)\,\alpha_{2J_\beta}^B(i\omega)\,d\omega + \delta X_1^{11}\,\delta_{J_\beta,1}, \\ \delta X_1^{11} &= \frac{3}{2}\left|\left\langle {}^3P_1^o\right||Q||\left.{}^3P_1^o\right\rangle\right|^2\alpha_1^A(0). \end{aligned} \tag{A1}$$

For $k = 2$, we have $J_\alpha = 2$ and $J_\beta = 0,1,2$. The coefficients $A_2^{2J_\beta}(\Omega)$ are listed in Table V. The quantities $X_2^{2J_\beta}$ are given by

$$\begin{aligned} X_2^{2J_\beta} &= \frac{45}{2\pi}\int_0^\infty \alpha_2^A(i\omega)\,\alpha_{1J_\beta}^B(i\omega)\,d\omega + \delta X_2^{20}\,\delta_{J_\beta,0}, \\ \delta X_2^{20} &= 2\left|\left\langle {}^3P_1^o\right||d||{}^1S_0\rangle\right|^2\sum_n \frac{\left(E_n - E_{{}^1S_0}\right)\left|\langle n||Q\right||{}^1S_0\rangle|^2}{\left(E_n - E_{{}^1S_0}\right)^2 - \omega_0^2}, \end{aligned} \tag{A2}$$

where $\omega_0 \equiv E_{{}^3P_1^o} - E_{{}^1S_0}$. For $k = 3$, we find that $J_\alpha = 1$ and $J_\beta = 1$. For all other J_α and J_β, this expression turns to zero. Then,

$$A_3^{11}(\Omega_p = 0) = (-1)^p\,3/5, \quad A_3^{11}(\Omega_p = 1) = (-1)^p\,1/5. \tag{A3}$$

$$X_3^{11} = \sum_{n,k}\left\langle {}^1S_0\right||d||\left.n\,{}^{1,3}P_1^o\right\rangle\left\langle n\,{}^{1,3}P_1^o\right||Q||\left.{}^3P_1^o\right\rangle\frac{\left\langle {}^3P_1^o\right||Q||\left.k\,{}^{1,3}P_1^o\right\rangle\left\langle k\,{}^{1,3}P_1^o\right||d||{}^1S_0\right\rangle}{E_n - E_{{}^1S_0} + E_k - E_{{}^3P_1^o}}. \tag{A4}$$

For $k = 4$, we have $J_\alpha = 2$ and $J_\beta = 2$. Then

$$A_4^{22}(\Omega_p = 0) = (-1)^p \frac{9}{25}; \quad A_4^{22}(\Omega_p = 1) = (-1)^p \frac{3}{25},$$

$$X_4^{22} = \sum_{n,k} \langle {}^1S_0||Q||n\,{}^{1,3}D_2\rangle\langle n\,{}^{1,3}D_2||d||{}^3P_1^o\rangle \frac{\langle {}^3P_1^o||d||k\,{}^{1,3}D_2\rangle\langle k\,{}^{1,3}D_2||Q||{}^1S_0\rangle}{E_n - E_{{}^1S_0} + E_k - E_{{}^3P_1^o}}. \tag{A5}$$

[1] N. D. Lemke, A. D. Ludlow, Z. W. Barber, T. M. Fortier, S. A. Diddams, Y. Jiang, S. R. Jefferts, T. P. Heavner, T. E. Parker, and C. W. Oates, Phys. Rev. Lett. **103**, 063001 (2009).

[2] Y. Takasu, K. Komori, K. Honda, M. Kumakura, T. Yabuzaki, and Y. Takahashi, Phys. Rev. Lett. **93**, 123202 (2004).

[3] A. V. Gorshkov, A. M. Rey, A. J. Daley, M. M. Boyd, J. Ye, P. Zoller, and M. D. Lukin, Phys. Rev. Lett. **102**, 110503 (2009).

[4] K. Tsigutkin, D. Dounas-Frazer, A. Family, J. E. Stalnaker, V. V. Yashchuk, and D. Budker, Phys. Rev. Lett. **103**, 071601 (2009).

[5] J. J. Hudson, D. M. Kara, I. J. Smallman, B. E. Sauer, M. R. Tarbutt, and E. A. Hinds, Nature (London) **473**, 493 (2011).

[6] E. R. Meyer and J. L. Bohn, Phys. Rev. A **80**, 042508 (2009).

[7] M. Borkowski, R. Ciuryło, P. S. Julienne, S. Tojo, K. Enomoto, and Y. Takahashi, Phys. Rev. A **80**, 012715 (2009).

[8] S. Tojo, M. Kitagawa, K. Enomoto, Y. Kato, Y. Takasu, M. Kumakura, and Y. Takahashi, Phys. Rev. Lett. **96**, 153201 (2006).

[9] K. Enomoto, M. Kitagawa, S. Tojo, and Y. Takahashi, Phys. Rev. Lett. **100**, 123001 (2008).

[10] M. Kitagawa, K. Enomoto, K. Kasa, Y. Takahashi, R. Ciuryło, P. Naidon, and P. S. Julienne, Phys. Rev. A **77**, 012719 (2008).

[11] R. Yamazaki, S. Taie, S. Sugawa, K. Enomoto, and Y. Takahashi, Phys. Rev. A **87**, 010704 (2013).

[12] Y. Takasu, Y. Saito, Y. Takahashi, M. Borkowski, R. Ciuryło, and P. S. Julienne, Phys. Rev. Lett. **108**, 173002 (2012).

[13] N. Nemitz, F. Baumer, F. Münchow, S. Tassy, and A. Görlitz, Phys. Rev. A **79**, 061403 (2009).

[14] F. Münchow, C. Bruni, M. Madalinski, and A. Görlitz, Phys. Chem. Chem. Phys. **13**, 18734 (2011).

[15] F. Baumer, F. Münchow, A. Görlitz, S. E. Maxwell, P. S. Julienne, and E. Tiesinga, Phys. Rev. A **83**, 040702 (2011).

[16] I. Reichenbach, P. S. Julienne, and I. H. Deutsch, Phys. Rev. A **80**, 020701 (2009).

[17] J. C. Sanders, O. Odong, J. Javanainen, and M. Mackie, Phys. Rev. A **83**, 031607 (2011).

[18] P. Julienne (private communication).

[19] M. S. Safronova, S. G. Porsev, and C. W. Clark, Phys. Rev. Lett. **109**, 230802 (2012).

[20] M. Marinescu and A. Dalgarno, Phys. Rev. A **52**, 311 (1995).

[21] M. Marinescu and H. R. Sadeghpour, Phys. Rev. A **59**, 390 (1999).

[22] J.-Y. Zhang and J. Mitroy, Phys. Rev. A **76**, 022705 (2007).

[23] A. Dalgarno and W. D. Davison, in *Advances in Atomic and Molecular Physics*, edited by D. Bates and I. Estermann (Academic, New York, 1966), Vol. 2, pp. 1–32.

[24] D. A. Varshalovich, A. N. Moskalev, and V. K. Khersonskii, *Quantum Theory of Angular Momentum* (World Scientific, Singapore, 1988).

[25] A. Dalgarno, *Quantum Theory*, Vol. 1 (Academic, New York, 1961).

[26] S. H. Patil and K. T. Tang, J. Chem. Phys. **106**, 2298 (1997).

[27] V. A. Dzuba, V. V. Flambaum, and M. G. Kozlov, Phys. Rev. A **54**, 3948 (1996).

[28] M. G. Kozlov, Int. J. Quantum Chem. **100**, 336 (2004).

[29] M. S. Safronova, M. G. Kozlov, W. R. Johnson, and D. Jiang, Phys. Rev. A **80**, 012516 (2009).

[30] M. S. Safronova, M. G. Kozlov, and C. W. Clark, Phys. Rev. Lett. **107**, 143006 (2011).

[31] S. A. Kotochigova and I. I. Tupitsyn, J. Phys. B: At. Mol. Opt. Phys. **20**, 4759 (1987).

[32] M. G. Kozlov and S. G. Porsev, Eur. Phys. J. D **5**, 59 (1999).

[33] Yu. Ralchenko, A. Kramida, J. Reader, and the NIST ASD Team (2011). NIST Atomic Spectra Database (version 4.1). Available at http://physics.nist.gov/asd.

[34] C. J. Bowers, D. Budker, S. J. Freedman, G. Gwinner, J. E. Stalnaker, and D. DeMille, Phys. Rev. A **59**, 3513 (1999).

[35] D. M. Bishop and J. Pipin, J. Chem. Phys. **97**, 3375 (1992).

[36] V. A. Dzuba and A. Derevianko, J. Phys. B: At. Mol. Opt. Phys. **43**, 074011 (2010).

[37] P. Zhang and A. Dalgarno, J. Phys. Chem. A **111**, 12471 (2007).

[38] B. K. Sahoo and B. P. Das, Phys. Rev. A **77**, 062516 (2008).

[39] S. G. Porsev and A. Derevianko, J. Chem. Phys. **119**, 844 (2003).